IEEE Access
Multidisciplinary | Rapid Review | Open Access Journal

Received November 13, 2018, accepted December 6, 2018, date of publication December 18, 2018,
date of current version January 11, 2019.

Digital Object Identifier 10.1109/ACCESS.2018.2887234

An Implantable Wideband Circularly Polarized Microstrip Patch Antenna via Two Pairs of Degenerate Modes

ZHI-JIE YANG[1], (Student Member, IEEE), LEI ZHU[2], (Fellow, IEEE), AND SHAOQIU XIAO[1], (Member, IEEE)

[1]School of Physics, Institute of Applied Physics, University of Electronic Science and Technology of China, Chengdu 610054, China
[2]Department of Electrical and Computer Engineering, Faculty of Science and Technology, University of Macau, Macau 999078, China

Corresponding author: Shaoqiu Xiao (xiaoshaoqiu@uestc.edu.cn)

This work was supported in part by the National Natural Science Foundation of China under Grant 61571468 and Grant 61731005, in part by the Pre-Research Foundation of National Defence under Grant 170441413086 and Grant 614240205070817, and in part by the Fundamental Research Funds for the Central Universities under Grant ZYGX2016Z008.

ABSTRACT This paper presents a design approach for developing a wideband circularly polarized (CP) microstrip patch antenna (MPA) embedded in the human body. To achieve this goal, a pair of high-order degenerate modes (TM_{30} and TM_{03}) in MPA have been excited and lowered for resonance in proximity to a pair of fundamental degenerate modes (TM_{10} and TM_{01}). The proper disturbance of these two pairs of radiative resonant modes can contribute to the generation of two CP radiating waves at two near-by operating frequencies, aiming to realize CP radiation in a wide operating band covered by these two frequencies. A novel implantable wideband CP MPA is proposed and developed due to the emergence of two minima in the axial-ratio (AR) frequency response. The designed MPA is then demonstrated to tremendously achieve the wide 3-dB AR bandwidth which covers the 2.4 to 2.48 GHz ISM-band in the cubic human skin model. Moreover, the proposed CP MPA shows good tolerance to the variety of tissue according to our study on sensitivity and model integrity. Finally, the designed CP MPA is fabricated and tested, and a good agreement exists between measured and simulated results in a wide frequency region.

INDEX TERMS Implantable antenna, circular polarization, wide bandwidth, lower and upper degenerate modes.

I. INTRODUCTION

Circularly polarized (CP) antennas are highly desired in implantable medical devices (IMDs) because of their attractive capability in reducing multipath interference and improving bit-error-rates against linear polarization (LP) for the wireless communication between in-body devices and external monitoring [1]–[3]. With unique dielectric properties, tissues of different individuals may have a huge influence on the radiated wave from an implantable antenna, thus causing the unexpected variation among them and the inevitable deviation of CP radiation of an in-body antenna embedded in different patients [4]–[6]. Intuitively speaking, these unexpected variations in CP radiation can be effectively compensated by an implantable CP antenna with wide 3-dB AR bandwidth.

In the past decades, many efforts have been devoted to designing and exploring various kinds of implantable CP antennas with wide 3-dB AR bandwidth [7]–[9]. For instance, a helix antenna with wide 3-dB AR bandwidth is firstly reported for a capsule [7]. A conformal wideband CP antenna has been recently designed for an endoscopic system. Herein, small perturbation achieves its impressive wide 3-dB AR bandwidth via the slots etched on the patch, and two helix long circumferences [8]. The internal space of the capsule has been effectively utilized by these antennas [7]–[9] which however unfortunately discomfort patients and find it so tough to be integrated with some specific IMDs like pacemaker due to the lack of available space.

Characterized by low profile, light weight, and easy fabrication, microstrip patch antenna (MPA) has been widely considered as a useful in-body antenna [10]. So far, an extensive investigation has been conducted on a single-fed MPA with wide 3-dB AR bandwidth [11]–[20]. A coaxial-fed MPA is firstly reported in [11] to achieve CP radiation through the installation of a pair of slight perturbation elements etched on one diagonal line of the patch. Due to the etching of the center slot on the patch, the proposed CP MPA has an extremely

large total quality factor (Q_T) so that only the fractional bandwidth (FBW) of 1.6% at around 2.4 GHz can be achieved by its 3-dB AR bandwidth [11]. Afterward, it is reported that a variety of CP MPAs based on this design concept has been developed one by one [12]–[20]. The widest 3-dB AR bandwidth achieves about 18.2% FBW among them, and this MPA operates at around 800 MHz [12]. Another MPA with 8.2% FBW at around 2.4 GHz is demonstrated by the work in [13]. It is necessary for both of two implantable CP MPAs to install center slots for miniaturization in size while introducing a pair of short pins for wideband CP radiation. In short, all of these reported implantable CP MPAs are developed through the perturbation of two near-by fundamental degenerate modes in a patch radiator. Recently, an alternative implantable CP MPA [19] has been developed by the formation of a pair of truncated elements and the increase of implant depth so as to effectively widen its 3-dB AR bandwidth through two distant fundamental degenerate modes. In general, only a pair of fundamental models like TM_{10} and TM_{01} in MPA have been employed by all of these reported works to realize CP radiation.

Next, a differentially-fed implantable MPA integrated with reactive loading is developed for the purpose of dual-band CP radiation [21]. The CP radiation in the lower band is attained by TM_{10} and TM_{01} modes whereas the CP radiation in the upper band is achieved by a pair of high-order degenerate modes like TM_{30} and TM_{03} [21]–[23]. In this paper, a new implantable CP MPA in the human body with extremely widened 3-dB AR bandwidth in one targeted working band will be presented by employing these two pairs of degenerate modes simultaneously.

The remainder of this paper is organized as follows. In Section II, a discussion will be held on the total quality factor (Q_T) of the CP MPA to show its extremely small value with slight variation in deep implantation. Then, an effective method is introduced to lower the resonant frequencies of TM_{30} and TM_{03}, which is aimed at widening 3-dB AR bandwidth by means of the high-loss tissue. To the authors' best knowledge, it is the first explicit attempt to accommodate these two pairs of degenerate modes for enhancing our concerned 3-dB AR bandwidth of a CP MPA embedded in the human body. In Section III, a single-fed implantable MPA with wider 3-dB AR bandwidth will be proposed and designed for the monitoring of the pacemaker operating at one of industrial, scientific and medical (ISM) bands, like 2.4 to 2.48 GHz. Next, sensitivity analysis will be carried out according to the variety of tissue to show the good tolerance of the proposed CP MPA. Meanwhile, a further study on model integrity will be conducted to evaluate the practicality of the proposed CP MPA. In Section IV, the measured results of the fabricated CP MPA are provided to validate the predicted ones. Finally, a conclusion is drawn in Section V.

II. PROPERTY OF HUMAN TISSUE

In fact, human body is a complicated environment for radio-frequency (RF) propagation. In contrast to free-space, most of human tissues have a variety of dielectric properties like high relative permittivity (ε_r) and conductivity (σ). For example, the ε_r and σ of human skin are 38.06 and 1.44 respectively at 2.45 GHz [13]. On the other hand, some kinds of human tissues are similar to normal materials. For instance, the ε_r and σ of human fat are only 5.28 and 0.1 respectively at 2.45 GHz. What's more, the dielectric properties of all human tissues are highly frequency-dependent, which may be dissimilar for various reasons such as age, weight, sex and health status [4]–[6]. In fact, the radiated performance of an implantable antenna is definitely and greatly affected by these variable dielectric properties of human tissue. Therefore, one key factor of an implantable MPA is its reliable stability of good radiation performance in a targeted frequency band. In this aspect, all human tissues have been exhibited to own a high loss tangent ($\tan\delta$) for RF signals [24] and [25], which has been employed to enhance the radiation performance of an implantable MPA [19].

Based on the above-mentioned description, it can be easily understood that the deviation of CP radiation can be effectively antagonized by an approach to widening 3-dB AR bandwidth. To achieve it, an approximate expression [26] for the relationship between Q_T and CP bandwidth (BW^{CP}) of a MPA can be deduced as follows:

$$BW^{CP} = 0.387/Q_T \tag{1}$$

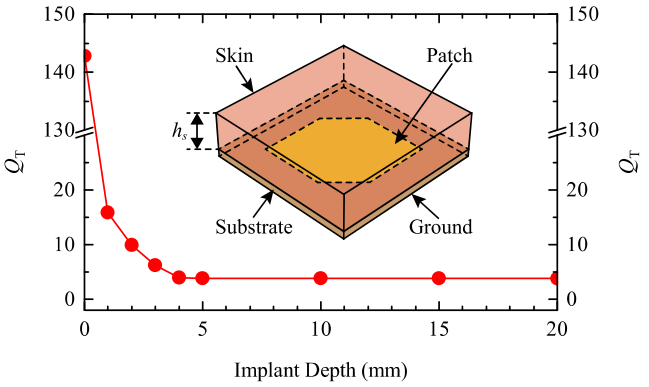

FIGURE 1. The calculated Q_T of MPA with different implant depths under the illustrated MPA geometry.

As shown in Eq. (1), CP bandwidth is inversely proportional to Q_T, which thus enhances CP bandwidth directly by the reduction of Q_T. In our previous work [19], the calculation process for the Q_T of an implantable CP MPA with shallow implant depth like $h_s \leq 4$ mm has been reported in detail, as illustrated in Fig. 1 with a simulated CP MPA model which is an ideal CP MPA loaded with human skin. In addition, a pair of truncated element is etched on the patch for CP radiation. The CP MPA is printed on a dielectric substrate like Rogers RO6010 with relatively high permittivity for the reduction of its physical size. Implant depth (h_s) is indicated in the transverse axis as shown in Fig. 1. At the starting point of 0 mm, a CP MPA model operates in the free-space without the loading of human tissue. As displayed from Fig. 1, Q_T sees a dramatic decline with the change of implant depth

in the case of $h_s \leq 4$ mm, which has been used to extend 3-dB AR bandwidth [19]. The Q_T with deep implantation ($h_s \geq 4$ mm) is obtained and illustrated in Fig. 1 by following the same calculation process, which suggests that the value of Q_T is extremely small and almost remains unchanged in the case of $h_s \geq 4$ mm. As such, Eq. (1) presents a fundamental limit for the enhancement of CP bandwidth due to extremely low and stable Q_T in deep implantation.

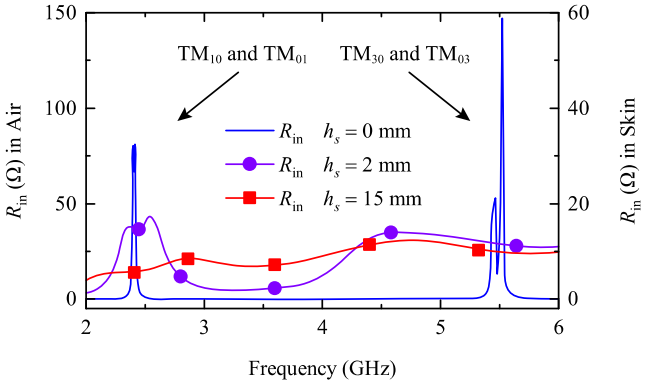

FIGURE 2. The calculated R_{in} of the MPA in Fig. 1 with different implant depths.

Very recently, an approach to simultaneously exciting fundamental mode (TM_{10}) and higher-order mode (TM_{30}) in a single patch radiator has been developed to effectively widen the impedance bandwidth in the air for linearly polarized (LP) radiation [27]–[30]. One of the difficulties in exciting these two resonant modes for LP radiation in the free-space lies in how to achieve good impedance matching over a wide band. The separate impedances of the simulated MPA model with different implant depths in Fig. 1 are presented in Fig. 2. It can be found from the blue curve in Fig. 2 that the separate impedances of the radiative modes of MPA working in the air see obvious changes. What' more, the huge difference between the input impedances of these two detached modes sees a decrease with the change of implant depth. The difference can be tremendously reduced by making use of the inherent high loss of human tissue due to the positive correlation between effective loss tangent and implant depth as discussed in [19], which thus makes it much easier to excite these modes in MPA for wideband radiation in the human body than in the air. Accordingly, we are allowed to come up with an idea to simultaneously excite and utilize two pairs of fundamental degenerate modes (TM_{10} and TM_{01}) and high-order degenerate modes (TM_{30} and TM_{03}) for wideband CP radiation via a perturbed patch radiator.

III. ANTENNA DESIGN AND DISCUSSION

A. SIMPLIFIED MODELS

As everyone knows, human body is a heterogeneous medium composed of multiple layers of human tissues with frequency-dependent dielectric properties. In order to speed up our design, a simplified model of human tissue is first preferred and referred as a single-layered tissue model [11]–[14] and [18]–[21]. In this context, a frequency-dependent one-layered skin model is offered in Fig. 3 and our proposed MPA is designed in this tissue model with a depth of h_s. The cubic human skin model has a dimension of 100 mm × 100 mm × (25 + h_s) mm.

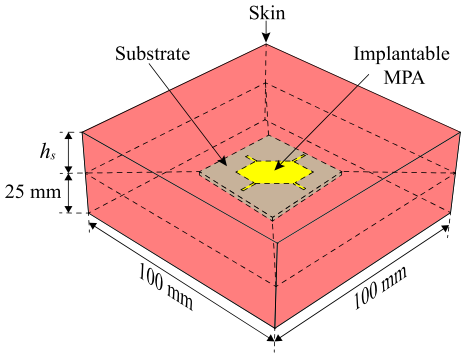

FIGURE 3. Schematic of the one-layered human skin model for characterization of the proposed implantable CP MPA.

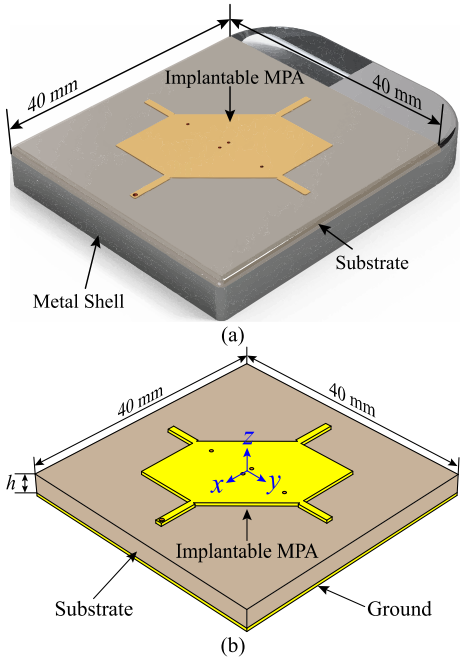

FIGURE 4. Demonstration of the proposed implantable wideband CP MPA. (a) Pacemaker integrated with a MPA, and (b) simplified model.

In the actual process of design, it is desired to take into account implantable antenna and its respective IMD. In this aspect, it is definitely preferred to take full advantage of existing conditions for designing such an implantable antenna with enhanced performance at maximum. For example, the metal shell of the pacemaker can be utilized as the ground plane of the MPA as discussed in [19]. Fig. 4(a) illustrates the detailed geometry of the pacemaker integrated with an implantable MPA. The thickness of metal shell has little effect on its radiation performance since the shell is electrically large enough to suppress the parasitic radiation from the edge of MPA. Thus, a simplified model with an infinitely thin ground plane as shown in Fig. 4(b) is used

herein for the simplification and acceleration of our simulation. In the simplified model, MPA is printed on the commercial Rogers RO6010 ($\varepsilon_r = 10.2$, $\tan\delta = 0.0023$) substrate with a thickness of $h = 0.635$ mm [11]–[21]. Meanwhile, the substrate is selected to have the same dimension with common pacemaker, like 40 mm × 40 mm [19]. For the sake of convenience, the center of the proposed implantable MPA is set as the origin of the coordinate system, as illustrated in Fig. 4(b).

B. WORKING PRINCIPLE AND SIMULATED RESULTS

An approach to simultaneously exciting fundamental modes (TM_{10} and TM_{01}) and higher-order modes (TM_{30} and TM_{03}) will be applied to widen the 3-dB AR bandwidth of an implantable MPA at 2.4-2.48 GHz ISM band for monitoring the pacemaker. The geometrical schematic of the proposed MPA is depicted in Fig. 5. As shown in Fig. 3, this MPA with an embedded depth of $h_s = 15$ mm is implanted in the one-layered skin model, whose detailed geometrical parameters are provided in Table 1. From Fig. 5, it can be seen that a pair of largely truncated areas are introduced for the realization of CP radiation by means of two perturbed degenerate modes under the condition of extremely low Q_T [19]. Meanwhile, two pairs of stubs with an equal width ($w_i = 1$ mm) are symmetrically printed along the four axes of the coordinate. The proposed MPA is fed by a coaxial probe with 50 Ω through one of the paired stubs along the x-axis. The feed point is 0.5 mm away from the edge.

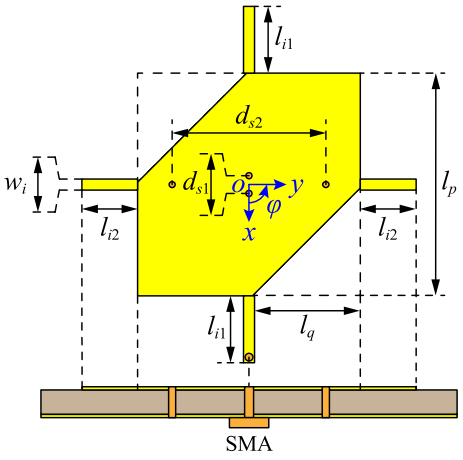

FIGURE 5. Geometrical schematic of the proposed CP MPA.

TABLE 1. Detailed dimensions of the proposed CP MPA in Fig. 5.

Parameters	l_p	l_q	l_{i1}	l_{i2}	w_i	d_{s1}	d_{s2}
Value (mm)	20	9.8	6	5	1	1.6	13.8

As displayed from Fig. 6, the simulated AR frequency response of the stub-loaded MPA is embedded in the skin model, which shows that the two pairs of stubs are used to reduce the CP operating frequencies of fundamental modes (f_{AR1}) and high-order modes (f_{AR3}). As such, f_{AR3} sees a dramatic drop. When $l_{i1} = 6$ mm, f_{AR1} and f_{AR3} are about

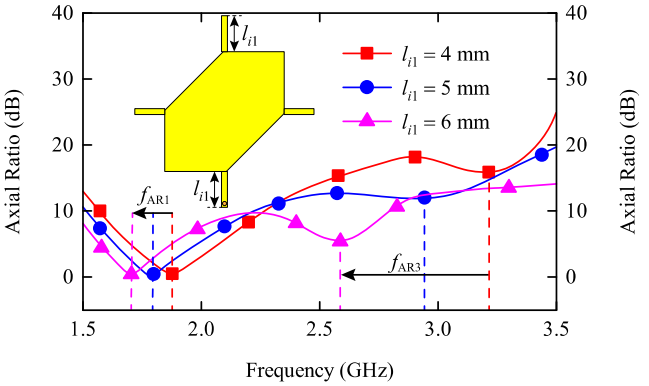

FIGURE 6. Simulated AR responses of the designed CP MPA with different l_{i1}.

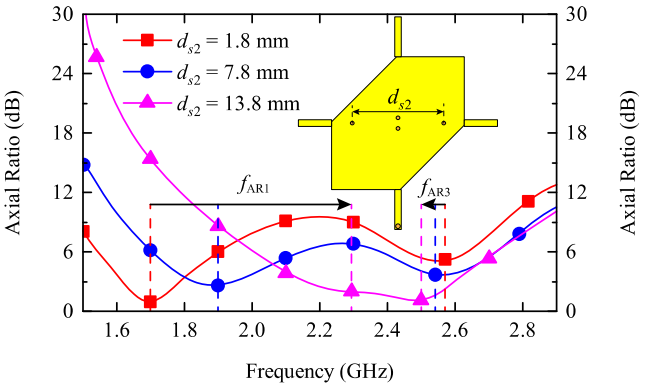

FIGURE 7. Simulated AR responses of the designed CP MPA with different d_{s2}.

1.7 GHz and 2.6 GHz, both of which appear outside the targeted 2.4-2.48 GHz ISM band. For the proper reallocation of f_{AR1} and f_{AR3} in proximity to each other, two pairs of shorting pins with an equal radius (0.5 mm) are further introduced and embedded in the substrate connecting the patch and ground plane, as displayed in Fig. 7. It can be seen from Fig. 7 that f_{AR1} sees a drastic increase by enlarging the gap between the two shorting pins along the y-axis while f_{AR3} witnesses a slight decrease. Furthermore, the AR in a range between f_{AR1} and f_{AR3} is continuously improved at the same time. Finally, a single-fed MPA with wide 3-dB AR bandwidth is designed to cover the 2.4-2.48 GHz ISM band for pacemaker monitoring system.

As shown in Fig. 8, the reflection coefficient ($|S_{11}|$) of the proposed CP MPA makes a simulated response. A wide impedance bandwidth is achieved under $|S_{11}| < -10$ dB in a range from 1.62 to 3.06 GHz (61.5% in fraction), thereby fully covering the 2.4-2.48 GHz ISM band as represented by the grey rectangle. As displayed from Fig. 9, the simulated AR response along the z-axis indicates that the AR below 3-dB covers a frequency range from 2.15 to 2.60 GHz (19% in fraction), which thus attains the widest 3-dB AR bandwidth in the 2.4-2.48 GHz ISM band. In contrast to the previous works under the operation of a single operating frequency (f_{AR1}), the proposed CP MPA has two minima in the AR response

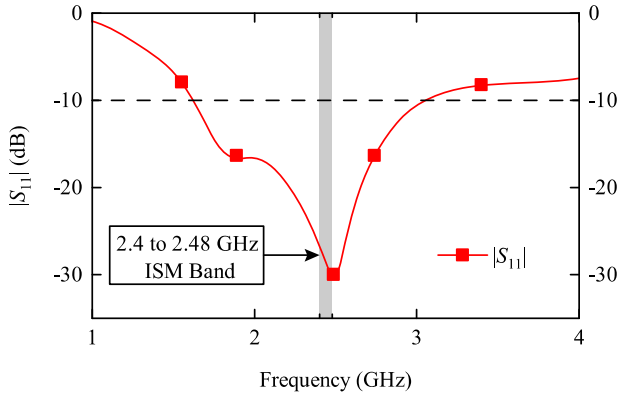

FIGURE 8. Simulated $|S_{11}|$ response of the proposed CP MPA.

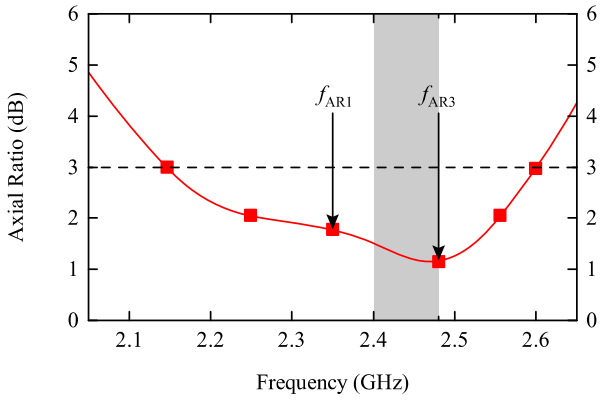

FIGURE 9. Simulated AR response of the proposed CP MPA in the one-layered skin model.

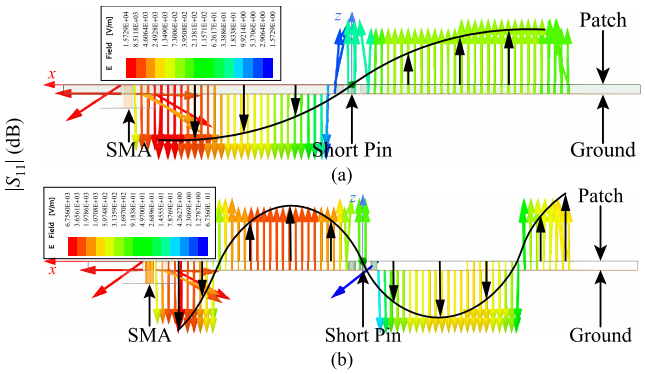

FIGURE 10. Distribution of electric fields underneath the radiating patch of the proposed CP MPA: (a) f_{AR1} and (b) f_{AR3}.

for CP radiation under the operation of two near-by operating frequencies at $f_{AR1} = 2.35$ GHz and $f_{AR3} = 2.48$ GHz. The widest 3-dB AR bandwidth is achieved by the connection of the two CP bands dominated by f_{AR1} and f_{AR3}.

Fig.10 shows the distribution of simulated electric fields underneath the radiating patch of the proposed implantable MPA at f_{AR1} and f_{AR3} respectively. The simulated and realized gain patterns at f_{AR1} and f_{AR3} are shown in Fig. 11. It can be seen from Fig. 11 that the proposed CP MPA which mainly radiates in the off-body direction has a peak gain of -22.5 dBi at boresight. As demonstrated in all

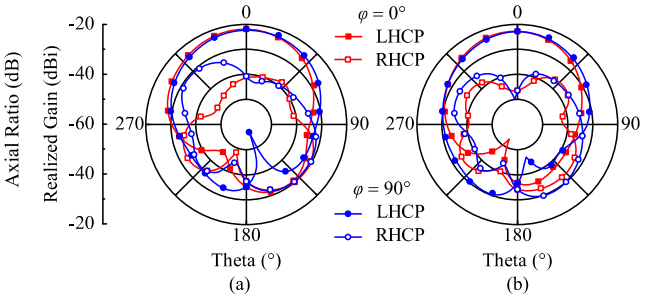

FIGURE 11. Realized gain patterns of the designed CP MPA in the *XZ*-plane ($\varphi = 0°$) and *YZ*-plane ($\varphi = 90°$): (a) f_{AR1} and (b) f_{AR3}.

reported implantable antennas, the negative gain in dB results from the high dissipation in the surrounding human tissue. In this design, a left-handed circular polarization (LHCP) with a cross-polarization discrimination of around 22 dB is achieved in the main radiation direction, which thus reveals high suppression over the unwanted right-handed circular polarization (RHCP).

C. SENSITIVITY ANALYSIS

As discussed above, human body is a heterogeneous media composed of multiple layers of human tissues with frequency-dependent dielectric properties. Definitely exerting a huge influence on the radiation performance of all implantable antennas, these variable properties may vary due to the unique feature of each individual. Thus, it is desired to evaluate the two important parameters including the $|S_{11}|$ and AR of the proposed CP MPA under a variety of tissue-loading conditions, namely variations of relative permittivity (ε_r), conductivity (σ) and implant depth (h_s).

The simulated $|S_{11}|$ responses of the proposed CP MPA are represented in Figs. 12 (a) and (b) when ε_r and σ of skin model are assumed to vary by $\pm 30\%$, while corresponding AR responses are illustrated in Figs. 13 (a) and (b) with the same variations. Apparently, the proposed implantable CP MPA can always operate in the targeted 2.4-2.48 GHz ISM band in spite of such variation in the dielectric properties of human tissue. As a result, it can be inferred that the proposed CP MPA shows attractive capability in those tolerances by virtue of its extremely widened AR bandwidth of CP radiation under the radiation of two pairs of degenerate modes or at dual operating frequencies, namely f_{AR1} and f_{AR3}.

Fig. 12(c) demonstrates the simulated $|S_{11}|$ of the proposed CP MPA in the range of h_s from 5 mm to 25 mm, which shows that resonance response is seldom affected by implant depth. Meanwhile, Fig. 13(c) illustrates the good operation of the CP radiation of the proposed antenna in the targeted frequency band despite a significant change in implant depth. Realistic biomedical application actually finds it difficult to precisely control the implant depth of IMDs within the level of millimeter magnitude. Therefore, high demands are set on the insensitivity of performances of the implantable MPA with respect to the implant depth. Compared with those previously-reported implantable CP MPAs,

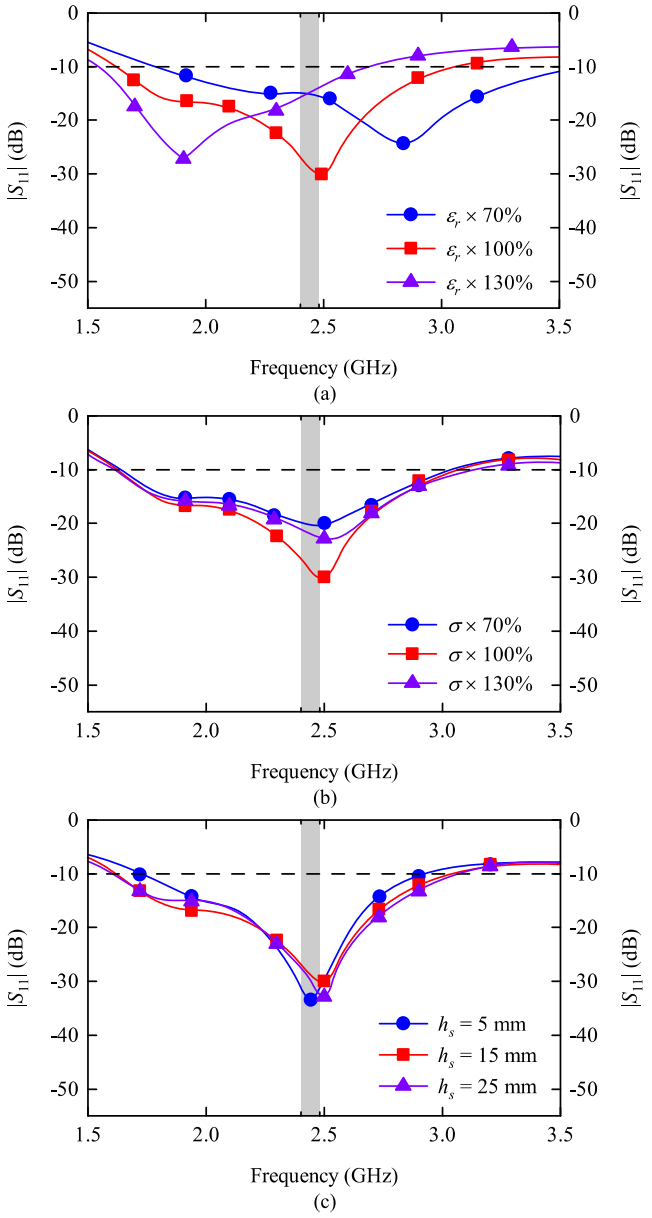

FIGURE 12. Simulated $|S_{11}|$ responses of the proposed CP MPA under varied ε_r , σ, and h_s. (a) ε_r of skin varies by ±30%, (b) σ of skin varies by ±30%, and (c) h_s varies from 5 mm to 25 mm.

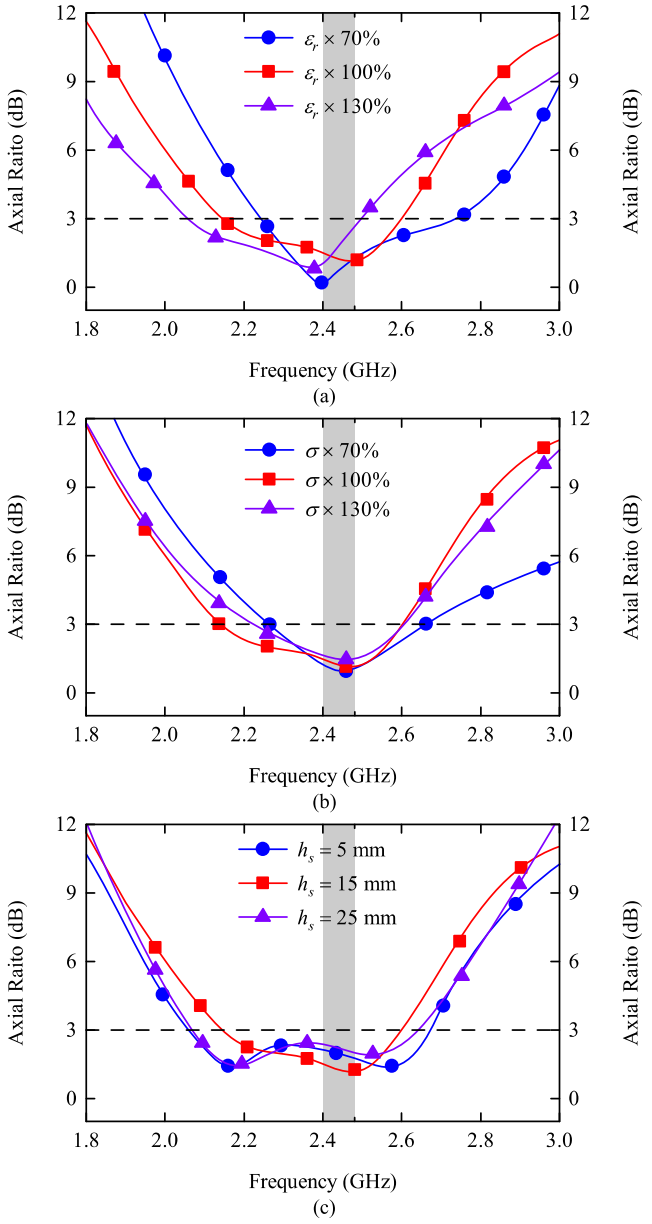

FIGURE 13. Simulated AR responses of the proposed CP MPA under varied ε_r , σ, and h_s. (a) ε_r of skin varies by ±30%, (b) σ of skin varies by ±30%, and (c) h_s varies from 5 mm to 25 mm.

our proposed implantable CP MPA shows a much larger tolerance to the variation of the tissue because the proposed method can make the best of the inherent high-loss feature of human body.

D. MODEL INTEGRITY STUDY

Hereinbefore, a simplification of pacemaker and human body has been conducted in order to facilitate our analysis and simulation. In practice, the implantable antenna should be designed with an actual IMD in an anatomical human body model. A much complicated but accurate model is displayed in Fig. 14(a) to observe the radiation performance of the designed CP MPA assembled with a realistic pacemaker. Herein, the pacemaker is modeled as a hollow metal cavity filled with such necessary electronic components as battery and circuitry. The whole shell has a fixed thickness of 10 mm. In addition, an insulating layer is used for the isolation of human tissue from direct contact with the metal MPA. Because of its electrical properties ($\varepsilon_r = 28$, $\tan\delta = 0$), zirconia is selected as a good material for biocompatible insulation from the perspective of magnetic field. The near-field of the implantable antenna is allowed by high relative permittivity and low loss-tangent values to be concentrated inside the low-loss encapsulation layer, which thus mitigates power loss [31]. The thickness of the superstrate is readily set to be 0.1 mm.

Hereafter, Fig. 14(b) shows the implantation of this complicated pacemaker model in the left chest of an anatomical

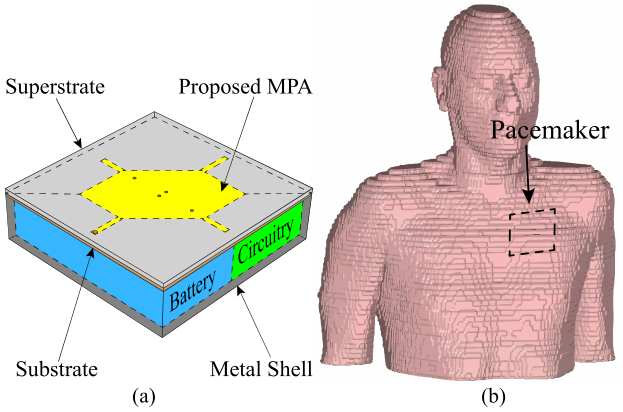

FIGURE 14. (a) Geometrical schematic of a pacemaker integrated with the proposed CP MPA, and (b) anatomical human body model.

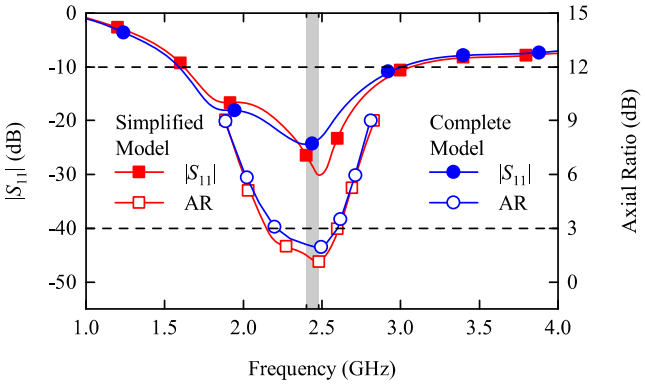

FIGURE 15. Simulated results of the proposed MPA obtained from two different models, namely simplified model and complete model.

human body model. Typically, pacemaker is implanted in a pocket formed between the skin and muscle of the upper chest area. Left-sided implants are more common for most of right-handed people, which can minimize the movement which is likely to occur because of arm movement [19]. As shown in Fig. 15, this complicated pacemaker model is remarked as "complete model", and "simplified model" represents the proposed CP MPA with an infinitely thin ground plane in the cubic one-layered skin model. Fig. 15 shows the simulated responses of $|S_{11}|$ and AR by means of two different models. As displayed from Fig. 15, the complexity of pacemaker model and human body model indeed has little effect on the radiation performances of the proposed CP MPA. The good accuracy of our presented approach is well verified by the good agreement between the simulated results obtained from different models.

E. SPECIFIC ABSORPTION RATE

To protect the safety of human being, two IEEE standards including C95.1-1999 and C95.1-2005 have been established to impose restrictions on specific absorption rate (SAR) levels [32]. Any designed implantable antenna should not exceed the specified levels of two IEEE standards, especially C95.1-1999 which is much tougher than C95.1-2005 [32]. In the first column of Table 2 is the simulated value of

TABLE 2. Simulated maximum SAR and maximum allowed input power of the proposed implantable CP MPA.

Maximum SAR (W/kg)		Maximum allowed net-input power (mW)	
1-g avg	10-g avg	C95.1-1999	C95.1-2005
194.2	33.5	8.2	59.7

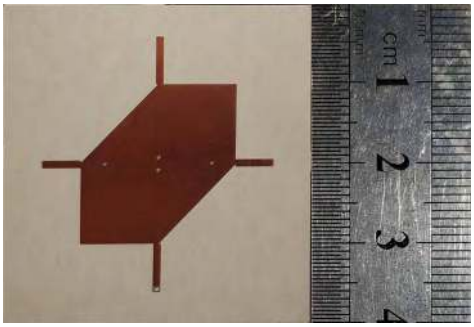

FIGURE 16. Photograph of the fabricated CP MPA with loading of four stubs.

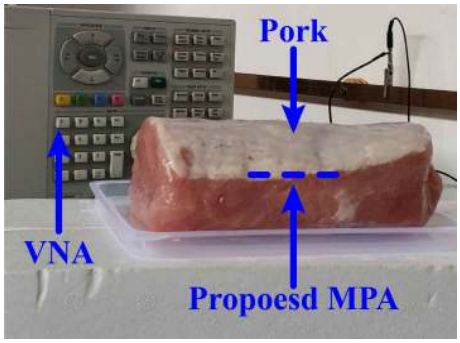

FIGURE 17. Photograph of experimental set-up for measuring the $|S_{11}|$ of the proposed CP MPA.

maximum averaged SAR in 1-g of human skin at 2.4 GHz, which is equal to 194.2 W/kg when the input power is 1 W. To abide by C95.1-1999, it is indicated by the third column of Table 2 that the proposed CP MPA in the one-layered skin model should have the maximum input power of less than 8.2 mW. Meanwhile, the simulated value of maximum averaged SAR in 10-g of human skin at 2.4 GHz is presented in the second column of Table 2 and equals 33.5 W/kg when the input power is 1 W. Thus, the proposed CP MPA in the one-layered skin model should have the maximum input power of less than 59.7 mW according to the C95.1-2005, as shown in the last column of Table 2.

IV. EXPERIMENTAL RESULTS AND VERIFICATIONS

The photograph of the fabricated antenna prototype is shown in Fig. 16. For the verification of the above-predicted radiation performances through experiment, this fabricated MPA is embedded in a cuboid pork, as displayed in Fig. 17. The proposed CP MPA is set to have an implant depth of about 15 mm. The inherent high-loss property of human body is conducive to fully realizing the wideband impedance and AR bandwidths of this CP MPA. Therefore, implant depth

has little impact on radiation performances in the case of the deep implantation of this CP MPA. As shown in Fig. 1, the reflection coefficient of the fabricated CP MPA is measured by Vector Network Analyzer (VNA) at the ambient temperature of 25 °C and under the relative humidity of 60%. Fig. 18 shows the measured result corresponding to the simulated one and a slight shift up in the measured frequency response compared with its simulated one.

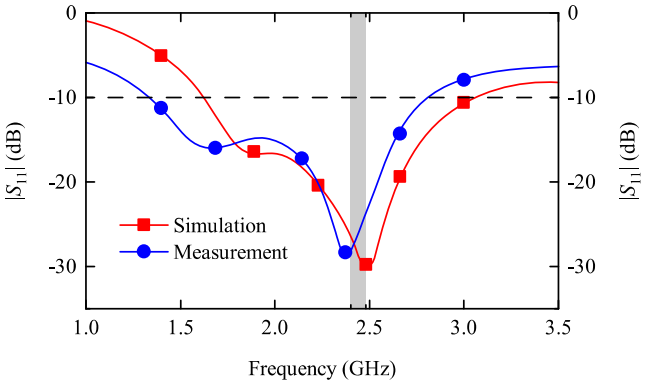

FIGURE 18. Simulated and measured $|S_{11}|$ responses of the proposed CP MPA.

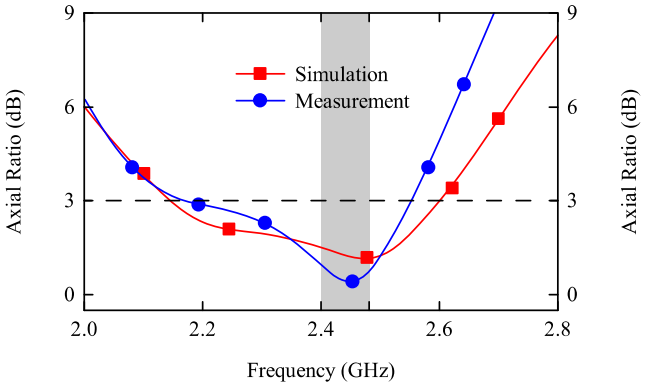

FIGURE 19. Simulated and measured AR responses of the proposed CP MPA.

Finally, the fabricated implantable wideband CP MPA is tested by the SATIMO near-field antenna measurement system, whose simulated and measured AR responses are displayed in Fig. 19. Fig. 19 indeed shows the emergence of two minima indeed in simulated and measured AR responses under the operation and radiation of two pairs of fundamental and high-order degenerate modes in a single patch radiator. Moreover, a reasonably good agreement exists between measured and simulated results over a wide frequency range.

V. CONCLUSION

An effective method has been proposed in this paper to develop an implantable CP MPA with much-widened impedance and AR bandwidths through simultaneously exciting two pairs of degenerate modes in a single patch radiator. A wide AR bandwidth with two minima in its frequency response has been achieved by lowering the resonant frequency of two high-order degenerate modes (TM_{30} and TM_{03}) towards that of the fundamental modes (TM_{10} and TM_{01}) and installing the perturbation of loaded stubs, short pins and truncated areas. Meanwhile, the inherent high-loss property of human body has been utilized to cause slight variation in its very small and stable input impedance, thus allowing us to excite these two pairs of degenerate modes for wideband CP radiation with no difficulty. Based on this method, an implantable wideband CP MPA operating in the 2.4-2.48 GHz ISM band has been designed to exhibit its widest 3-dB AR bandwidth among all the reported ones. Furthermore, the sensitivity analysis of the embedded environment indicates the good tolerance of our proposed CP antenna to the variation of dielectric properties of human tissue and the little impact of implant depth on radiated performances due to the inherent high loss of human tissue. After a simplified model is used to confirm the simulated results of the proposed CP MPA integrated with a complete pacemaker model in an anatomy human model, a prototype antenna is fabricated and tested for the evident verification of simulated results in a wideband frequency range.

REFERENCES

[1] W. Lei, H. Chu, and Y.-X. Guo, "Design of a circularly polarized ground radiation antenna for biomedical applications," *IEEE Trans. Antennas Propag.*, vol. 64, no. 6, pp. 2535–2540, Jun. 2016.
[2] Y.-X. Guo and C. Liu, "Miniaturized implantable circularly polarized patch antenna," in *Proc. iWEM*, Sapporo, Japan, Aug. 2014, pp. 271–272.
[3] C. Liu, Y.-X. Guo, and S. Xiao, "Small circularly polarized implantable antennas," in *Proc. iWEM*, Kowloon, China, Aug. 2013, pp. 20–22.
[4] N. Vidal, S. Curto, J. M. Lopez-Villegas, J. Sieiro, and F. M. Ramos, "Detuning effects on implantable antenna at various human positions," in *Proc. 6th EUCAP*, Prague, Czech Republic, Mar. 2012, pp. 1231–1234.
[5] N. Vidal, S. Curto, J. M. Lopez Villegas, J. Sieiro, and F. M. Ramos, "Detuning study of implantable antennas inside the human body," *Prog. Electromagn. Res.*, vol. 124, pp. 265–283, Jan. 2012.
[6] C. M. Furse, "Biomedical telemetry: Today's opportunities and challenges," in *Proc. IWAT*, Santa Monica, CA, USA, Mar. 2009, pp. 1–4.
[7] C. Liu, Y.-X. Guo, and S. Xiao, "Circularly polarized helical antenna for ISM-band ingestible capsule endoscope systems," *IEEE Trans. Antennas Propag.*, vol. 62, no. 12, pp. 6027–6039, Dec. 2014.
[8] R. Das and H. Yoo, "A wideband circularly polarized conformal endoscopic antenna system for high-speed data transfer," *IEEE Trans. Antennas Propag.*, vol. 65, no. 6, pp. 2816–2826, Jun. 2017.
[9] Z. Duan and L.-J. Xu, "Dual-band implantable antenna with circular polarisation property for ingestible capsule application," *Electron. Lett.*, vol. 53, no. 16, pp. 1090–1092, Aug. 2017.
[10] X. Zhang and L. Zhu, "Gain-enhanced patch antennas with loading of shorting pins," *IEEE Trans. Antennas Propag.*, vol. 64, no. 8, pp. 3310–3318, Aug. 2016.
[11] C. Liu, Y.-X. Guo, and S. Xiao, "Capacitively loaded circularly polarized implantable patch antenna for ISM band biomedical applications," *IEEE Trans. Antennas Propag.*, vol. 62, no. 5, pp. 2407–2417, May 2014.
[12] L. J. Xu, Y. X. Guo, and W. Wu, "Miniaturized circularly polarized loop antenna for biomedical applications," *IEEE Trans. Antennas Propag.*, vol. 63, no. 3, pp. 922–930, Mar. 2015.
[13] Z.-J. Yang, S.-Q. Xiao, L. Zhu, B.-Z. Wang, and H.-L. Tu, "A circularly polarized implantable antenna for 2.4-GHz ISM band biomedical applications," *IEEE Antennas Wireless Propag. Lett.*, vol. 16, pp. 2554–2557, 2017.
[14] H. Li, Y.-X. Guo, and S. Xiao, "A wideband implantable antenna with circularly polarization," in *Proc. IMWS-AMP*, Suzhou, China, Jul. 2015, pp. 1–3.
[15] C. Liu, Y. Zhang, and X. Liu, "Circularly polarized implantable antenna for 915 MHz ISM-band far-field wireless power transmission," *IEEE Antennas Wireless Propag. Lett*, vol. 17, no. 3, pp. 373–376, Mar. 2018.

[16] C. Liu, Y. X. Guo, R. Jegadeesan, and S. Xiao, "*In vivo* testing of circularly polarized implantable antennas in rats," *IEEE Antennas Wireless Propag. Lett.*, vol. 14, pp. 783–786, 2015.
[17] J. Li, T. Chang, and X. Liu, "A compact circularly polarized antenna for in-body wireless communications," in *Proc. IEEE Int. Symp. Antennas Propag. USNC/URSI Nat. Radio Sci. Meeting*, San Diego, CA, USA, Jul. 2017, pp. 2593–2594.
[18] B. Li and X.-Y. Liu, "A differentially fed implantable antenna with circularly polarization for biomedical telemetry," in *Proc. ICCEM*, Guangzhou, China, Feb. 2016, pp. 364–366.
[19] Z.-J. Yang, L. Zhu, and S. Xiao, "An implantable circularly polarized patch antenna design for pacemaker monitoring based on quality factor analysis," *IEEE Trans. Antennas Propag.*, vol. 66, no. 10, pp. 5180–5192, Oct. 2018.
[20] Y. Zhang, C. Liu, X. Liu, K. Zhang, and X. Yang, "A wideband circularly polarized implantable antenna for 915 MHz ISM-band biotelemetry devices," *IEEE Antennas Wireless Propag. Lett*, vol. 17, no. 8, pp. 1473–1477, Aug. 2018.
[21] X. Yang, X. Liu, and B. Li, "A dual-band circularly polarized antenna with differential feeding for implanted bio-sensors," in *Proc. ICCEM*, Guangzhou, China, Feb. 2016, pp. 197–199.
[22] J.-D. Zhang, L. Zhu, N.-W. Liu, and W. Wu, "Dual-band and dual-circularly polarized single-layer microstrip array based on multiresonant modes," *IEEE Trans. Antennas Propag.*, vol. 65, no. 3, pp. 1428–1433, Mar. 2017.
[23] J.-D. Zhang, L. Zhu, N.-W. Liu, and W. Wu, "CP patch antenna with controllable polarisation over dual-frequency bands," *IET Microw., Antennas Propag.*, vol. 11, no. 2, pp. 224–231, Jan. 2017.
[24] P. Turalchuk, I. Munina, V. Pleskachev, V. Kirillov, O. Vendik, and I. Vendik, "In-body and on-body wave propagation: Modeling and measurements," in *Proc. iWAT*, Athens, Greece, Mar. 2017, pp. 154–157.
[25] D. Kurup, W. Joseph, G. Vermeeren, and L. Martens, "In-body path loss model for homogeneous human tissues," *IEEE Trans. Electromagn. Compat.*, vol. 54, no. 3, pp. 556–564, Jun. 2012.
[26] D. R. Jackson, "Microstrip antennas," in *Antenna Engineering Handbook*, New York, NY, USA: McGraw-Hill, 1984.
[27] N.-W. Liu, L. Zhu, and W.-W. Choi, "A differential-fed microstrip patch antenna with bandwidth enhancement under operation of $TM_{10}$and TM_{30}modes," *IEEE Trans. Antennas Propag.*, vol. 65, no. 4, pp. 1607–1614, Apr. 2017.
[28] N.-W. Liu, L. Zhu, W.-W. Choi, and J.-D. Zhang, "A low-profile aperture-coupled microstrip antenna with enhanced bandwidth under dual resonance," *IEEE Trans. Antennas Propag.*, vol. 65, no. 3, pp. 1055–1062, Mar. 2017.
[29] N.-W. Liu, L. Zhu, W.-W. Choi, and J.-D. Zhang, "A novel differential-fed patch antenna on stepped-impedance resonator with enhanced bandwidth under dual-resonance," *IEEE Trans. Antennas Propag.*, vol. 64, no. 11, pp. 4618–4625, Nov. 2016.
[30] N.-W. Liu, L. Zhu, W.-W. Choi, and X. Zhang, "Wideband shorted patch antenna under radiation of dual-resonant modes," *IEEE Trans. Antennas Propag.*, vol. 65, no. 6, pp. 2789–2796, Jun. 2017.
[31] F. Merli, B. Fuchs, J. R. Mosig, and A. K. Skrivervik, "The effect of insulating layers on the performance of implanted antennas," *IEEE Trans. Antenna Propag.*, vol. 59, no. 1, pp. 21–31, Jan. 2011.
[32] C. Liu, Y.-X. Guo, H. Sun, and S. Xiao, "Design and safety considerations of an implantable rectenna for far-field wireless power transfer," *IEEE Trans. Antennas Propag.*, vol. 62, no. 11, pp. 5798–5806, Nov. 2014.

ZHI-JIE YANG (S'17) was born in Sichuan, China, in 1990. He received the B.S. degree in physics from Sichuan Normal University, Chengdu, China, in 2012. He is currently pursuing the Ph.D. degree in radio physics with the University of Electronic Science and Technology of China, Chengdu, China. In 2017, he was with the University of Macau, Macau, China, as a Research Assistant. His current research interests include microstrip antenna and implantable antenna.

LEI ZHU (S'91–M'93–SM'00–F'12) received the B.Eng. and M.Eng. degrees in radio engineering from the Nanjing Institute of Technology (now Southeast University), Nanjing, China, in 1985 and 1988, respectively, and the Ph.D. Degree in electronic engineering from the University of Electro-Communications, Tokyo, Japan, in 1993.

From 1993 to 1996, he was a Research Engineer with Matsushita-Kotobuki Electronics Industries Ltd., Tokyo. From 1996 to 2000, he was a Research Fellow with the École Polytechnique de Montréal, Montréal, QC, Canada. From 2000 to 2013, he was an Associate Professor with the School of Electrical and Electronic Engineering, Nanyang Technological University, Singapore. He joined the Faculty of Science and Technology, University of Macau, Macau, China, as a Full Professor, in 2013, where he has been a Distinguished Professor, since 2016. From 2014 to 2017, he has served as the Head of the Department of Electrical and Computer Engineering, University of Macau. So far, he has authored or co-authored over 465 papers in international journals and conference proceedings. His papers have been cited over 5900 times with a H-index of 41 (source: ISI Web of Science). His research interests include microwave circuits, guided-wave periodic structures, planar antennas, and computational electromagnetic techniques.

Dr. Zhu was a recipient of the 1997 Asia-Pacific Microwave Prize Award, the 1996 Silver Award of Excellent Invention from Matsushita-Kotobuki Electronics Industries Ltd., and the 1993 First-Order Achievement Award in Science and Technology from the National Education Committee, China. He served as a Member of the IEEE MTT-S Fellow Evaluation Committee (2013–2015), and has been serving as a Member of the IEEE AP-S Fellows Committee (2015–2017). He served as the General Chair of the 2008 IEEE MTT-S International Microwave Workshop Series on the Art of Miniaturizing RF and Microwave Passive Components, Chengdu, China, and the Technical Program Committee Co-Chair of the 2009 Asia-Pacific Microwave Conference, Singapore. He was an Associate Editor of the IEEE TRANSACTIONS ON MICROWAVE THEORY AND TECHNIQUES (2010–2013) and the IEEE MICROWAVE AND WIRELESS COMPONENTS LETTERS (2006–2012).

SHAOQIU XIAO (M'05) received the Ph.D. degree in electromagnetic field and microwave technology from the University of Electronic Science and Technology of China (UESTC), Chengdu, China, in 2003. In 2004, he joined UESTC as an Assistant Professor. From 2004 to 2006, he worked for the Wireless Communications Laboratory, National Institute of Information and Communications Technology of Japan, Singapore, as a Research Fellow, with a focus on the planar antenna and smart antenna design and optimization. From 2006 to 2010, he was with UESTC as an Associate Professor, where he is currently a Professor. He visited Ecole Normale Superieure de Cachan, Paris, France, as a Senior Research Scholar, in 2015. He has authored/co-authored over 300 technical journals, conference papers, books, and book chapters. His current research interests include planar antenna and phased array, computational electromagnetics, microwave passive circuits, and time reversal electromagnetics.